A Prognostics Framework for Battery Health Monitoring Integrated with Thermal Modeling

Chetan Kulkarni* and Mohit Mehta.†
KBR Inc, Intelligent Systems Division, NASA Ames Research Center, Moffett Field, CA 94035

Michael Khasin‡and John W. Lawson.§
Intelligent Systems Division, NASA Ames Research Center, Moffett Field, CA 94035

Urban Air Mobility (UAM) promises to revolutionize transportation in major cities, offering passenger travel, cargo delivery, and emergency medical services through a network of electric vertical takeoff and landing (eVTOL) aircraft. However, the limited range of current eVTOLs, due to the low specific energy of lithium-ion batteries along with a possibility of thermal runaway conditions poses significant safety concerns, leading to potentially compromising operational safety.

To address this critical challenge, researchers are actively evaluating the impact of flight and environmental conditions on onboard lithium-ion battery health. This involves carefully assessing the performance of battery packs under laboratory and operational conditions for developing models to estimate future health using prognostics framework.

This study examines the effectiveness of evaluating battery degradation leading to catastrophic failures under varying operational conditions in laboratory. These are captured using physics based models of underlying phenomenons and integrated into the prognostics framework. A fully charged battery undergoes controlled discharge cycles at varying C-rates based on the simulated power draw profile, with current and voltage, temperature data recorded throughout the experiment. The observed data provides valuable insights into how different operating conditions and mission profiles affect battery performance. This information is crucial for developing strategies to optimize battery systems, enhance range, and ultimately ensure the safe and reliable operation of UAM vehicles.

Nomenclature

Li-Po	=	Lithium-ion polymer battery
SOC	=	State-of-charge of the onboard lithium-ion polymer battery pack
EOD	=	End-of-discharge of the onboard lithium-ion polymer battery pack
V(t)	=	Voltage of the onboard lithium-ion polymer battery pack
Li-ion	=	Lithium-ion
OCP	=	Open Circuit Potential
PHM	=	Prognostics and Health Management
RMSE	=	Root Mean Square Error
RUL	=	Remaining Useful Life
SEI	=	Solid Electrolyte Interphase
SFP	=	Simulated Flight Profile
EOF	=	End of Flight

*Scientist, Intelligent Systems Division, and AIAA Associate Fellow.
†Scientist, Intelligent Systems Division, and AIAA Senior Member
‡Aerospace Engineer, Intelligent Systems Division.
§Senior Scientist, Intelligent Systems Division, and AIAA Senior Member

I. Introduction

Recent technological advances have made it possible to build and test experimental flights for electric Vertical Takeoff and Landing (eVTOL) aircraft [1–3]. Several companies such as Airbus A^3, Aurora Flight Sciences, EHang, Joby Aviation, Kitty Hawk, Leonardo, Lilium, Terrafugia and Volocopter are developing different types of eVTOL aircraft [3]. They all employ distributed electric propulsion (DEP) systems [2]. The low specific energy of current lithium-ion polymer (Li-Po) battery technology used for powering DEP system constrains the range of flight. Limited range has safety impact due to the reduced amount of time available for the pilot to assess the situation and take corrective actions, and for flying to an alternative landing area or returning to the origin in emergency situations. An important area of research therefore is accurate prediction of the state of the onboard Li-Po battery pack for safety margin assessment for continuation of the mission or for invoking contingencies.

This work integrates computed power demand obtained from the trajectory simulation of a quad-rotor vehicle and engineered down into a hardware-in-loop test with a single cell simulation for observing electrical and thermal battery characteristics. The power demand values are normalized to a single 18650 type cell for performing the experiments.

Ensuring safety in electric aviation is critical, as aircraft performance is significantly affected by battery weight compared to electric vehicles. Ongoing research prioritizes optimizing battery packs, individual cells, fire suppression systems, thermal management, and protective enclosures to maximize safety. [4–7]. .

Incorporating early warning systems in electric aviation can alleviate the challenges of developing ultra-safe batteries. Early warning, in this case, refers to detecting a potential cell failure before the next scheduled maintenance or after a specific number of flights. This proactive approach enables the timely removal of the faulty cell, preventing thermal runaway and eliminating the need to contain its spread to neighboring cells [8].

In this work, a model based prognostics framework integrating physics-based model for li-ion batteries integrated with a thermal model is presented to demonstrate future estimation of the battery thermal profile based on loading conditions. This will enable the decision making tools either human-in-loop or autonomous systems, to take specific decisions based on safety requirements.

The remainder of this manuscript is organized as follows: Section II details the development of the electro-chemical and thermal models. Section III presents a generalized prognostics architecture incorporating the updated thermal model. Section IV discusses validation of the developed model through three case studies. Section V provides a brief overview of the ProgPy open-source toolkit, which integrates the developed model. Finally, Section VI concludes the manuscript with key takeaways and potential future work.

II. Battery Model Development

A lumped-parameter ordinary differential equation model of Li-ion 18650 battery cells [9] is used as reference in this work. This model efficiently captures key electrochemical processes, accurately predicting state-of-charge (SOC) and end-of-discharge (EOD) voltage. The model and its associated prognostics algorithms have been previously validated on electric UAVs [10].

The model computes cell voltage over time based on current draw, considering various electrochemical factors. It uses a simplified form that maintains accuracy while remaining computationally efficient for real-time prognostics. Though tailored for Li-ion 18650 batteries with a nominal voltage of 3.7V and capacity of 2200mAh, the model's structure can be adapted for other battery chemistries in the generalized form.

The voltages of a battery are summarized in Fig. 1 [9]. The overall battery voltage $V(t)$ is the difference between the potential at the positive current collector, $\phi_s(0,t)$, and the negative current collector, $\phi_s(L,t)$, minus resistance losses at the current collectors (not shown in the diagram). As shown in the figure, the potentials vary with the distance $d \in [0, L]$, because the loss varies with distance from the current collectors.

The potentials at the current collectors are described by several voltage terms. The equilibrium potential at the positive current collector is $V_{U,p}$. This voltage is reduced by $V_{s,p}$, due to the solid-phase ohmic resistance, and $V_{\eta,p}$, the surface overpotential. The electrolyte ohmic resistance then causes another drop V_e. At the negative electrode, there is a drop $V_{\eta,n}$ due to the surface overpotential, and a drop $V_{s,n}$ due to the solid-phase resistance. The voltage drops again due to the equilibrium potential at the negative current collector $V_{U,n}$.

In theory, each cell reaches a voltage of around 4.2 V when fully charged. The battery's terminal voltage increases or decreases during charging and discharging, respectively. At the end of each cycle, it stabilizes at a steady-state voltage depending on its state of charge (SOC). By convention, SOC is defined as 1 when the battery reaches its full charge of 4.2 V and 0 when fully discharged. Therefore, even in a degraded battery, the SOC for maximum charge remains 1 by definition.

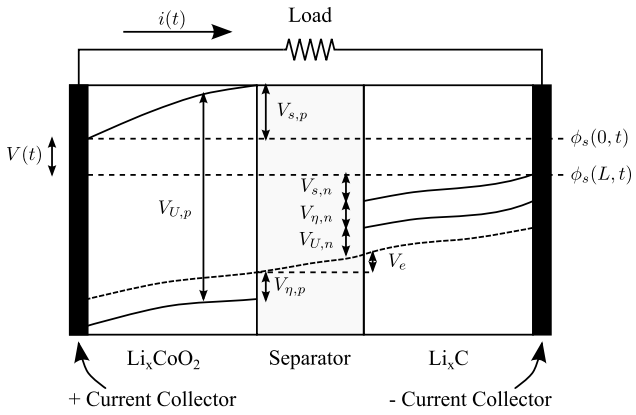

Fig. 1 Li-ion battery internal voltages.[9]

In this model, the state of charge (SOC) is represented by a variable analogous to the mole fraction x_n but scaled from 0 to 1. The model distinguishes between two types of SOC: nominal and *apparent*. Nominal SOC considers both the bulk and surface layers of the negative electrode, reflecting the total number of ions present. Apparent SOC, however, only considers the surface layer. Therefore, a battery discharged at a given rate can reach a predefined voltage cutoff, meaning its apparent SOC becomes 0. In this study, we set the apparent SOC threshold for predicting the end-of-discharge at 40%.

But, once the concentration gradient settles out, the surface layer will be partially replenished and the battery can be discharged further, i.e, apparent SOC increases whereas nominal SOC remains the same.

A. State of Charge

The State of Charge (SOC) of a battery is traditionally defined as 1 when fully charged and 0 when fully discharged. In this model, it's similar to the mole fraction x_n, but scaled from 0 to 1. However, there's a distinction between nominal SOC and apparent SOC. Nominal SOC is calculated based on both bulk and surface layer CVs in the negative electrode, while apparent SOC is determined solely by the surface layer. This means a battery can be discharged at a certain rate, hitting the voltage cutoff (apparent SOC of 0). Yet, once the concentration gradient stabilizes, the surface layer partially replenishes, allowing for further discharge. Thus, apparent SOC increases while nominal SOC stays constant.

Nominal (n) and apparent (a) SOC can then be defined using

$$SOC_n = \frac{q_n}{0.6q^{\max}} \tag{1}$$

$$SOC_a = \frac{q_{s,n}}{0.6q^{\max_{s,n}}}, \tag{2}$$

where $q^{\max_{s,n}} = q^{\max}\frac{v_{s,n}}{v_n}$. The factor $1/0.6$ comes from the fact that the mole fraction at the positive electrode cannot go below 0.4, therefore SOC of 1 corresponds to the point where $q_n = 0.6q^{\max_{s,n}}$.

B. Battery Voltage

The battery voltage are expressed as below to incorporate all the internal voltages within.

$$V = V_{U,p} - V_{U,n} - V_o - V_{\eta,p} - V_{\eta,n}. \tag{3}$$

Voltages in the battery are not observed to change instantaneously, i.e., the voltage changes occur smoothly. When discharge completes, for example, the voltage rises slowly as the surface layers move to the concentrations of the bulk volumes, as caused by diffusion. In addition to this, there are transients associated with V_o and the $V_{\eta,i}$ terms. To take this into account in a simple way, we compute voltage using

$$V = V_{U,p} - V_{U,n} - V'_o - V'_{\eta,p} - V'_{\eta,n}, \tag{4}$$

where

$$\dot{V}'_o = (V_o - V'_o)/\tau_o \tag{5}$$
$$\dot{V}'_{\eta,p} = (V_{\eta,p} - V'_{\eta,p})/\tau_{\eta,p} \tag{6}$$
$$\dot{V}'_{\eta,n} = (V_{\eta,n} - V'_{\eta,n})/\tau_{\eta,n}, \tag{7}$$

where the τ parameters are empirical time constants.

The model contains as states $\mathbf{x}$, $q_{s,p}$, $q_{b,p}$, $q_{b,n}$, $q_{s,n}$, V'_o, $V'_{\eta,p}$, and $V'_{\eta,n}$. The single model output is V. Model parameters are given for cell discussed in details in [11]

C. Thermal Modeling

The Li-ion cells used in this work are of 18650 type, for such geometries, the thermal diffusion time across the cell is much shorter than the characteristic cooling time [12, 13]. For this geometry and structure the temperature distribution across the cell is approximated by a uniform distribution [6, 7, 14].

An assumption of small temperature variation is considered between the battery cell and its environment $\Delta T = T - T_a$, the heat flux leaving the cell is approximately proportional to that difference (unless radiation losses are significant [15]). This proportionality depends on the thermal properties of the battery materials and the effectiveness of heat transfer to the surrounding environment. This simplification leads to the following ordinary differential equation, which governs the temperature evolution within a cell subjected to variable current I(t) [16]

A lumped thermal model of a cell assumes that the rate of change of the temperature of the cell depends on a balance between the heating element and heat dissipation,

$$m_{\text{cell}} C_p \frac{dT}{dt} = \dot{Q}_{\text{source/sink}} - \dot{Q}_{\text{environment}} \tag{8}$$

where m_{cell} is the averaged mass of the cell and C_p is the averaged heat capacity, the heat generation term depends on various contributions in a battery,

$$\dot{Q}_{\text{source/sink}} = V_{\text{cell}} \left[q_{\Omega,\text{l}} + q_{\Omega,\text{s}} + q_{\text{irr,ec}} + q_{\text{irr,pl}} + q_{\text{irr,st}} + q_{\text{therm,ec}} + q_{\text{therm,pl}} + q_{\text{therm,st}} \right] \tag{9}$$

where V_{cell} is the volume of the cell (or the heating element being considered), $q_{\Omega,\text{l}}$ is the ohmic heat generated by the electrolyte, $q_{\Omega,\text{s}}$ is the heat generated by the solid components (current collector, metallic wires etc.), $q_{\text{irr,ec}}$ is the irreversible heat generated from the electrochemical reactions, $q_{\text{irr,pl}}$ is the irreversible heat generated due to lithium platting, $q_{\text{irr,st}}$ is the ohmic heat generated by a short circuit, and q_{therm} is the thermodynamic heat from the electrochemical reactions and lithium plating, while the heat loss to a stationary fluid (air) is modeled through convection and radiation [15],

$$\dot{Q}_{\text{environment}} = h_{\text{conv}} A_{\text{cell}} \left(T_{\text{cell}} - T_{\text{amb}} \right) + \epsilon_{th} \sigma_B A_{\text{cell}} \left(T^4_{\text{cell}} - T^4_{\text{amb}} \right). \tag{10}$$

where T_{cell} is the surface temperature of a cell, T_{amb} is the ambient temperature, A_{cell} is the active cooling surface area, h_{conv} is the heat transfer coefficient, Note that this model assumes that the heat is generated in the cell's electrochemical core, the heat conduction between the core and the surface is extremely fast. The convective heat transfer coefficient can be calculated using $h = \frac{Nu \cdot k_{fluid}}{D_{hydraulic}}$, where k_{fluid} is the thermal conductivity, $D_{hydraulic}$ is the hydraulic diameter of the channel used to regulate the temperature using fluid, and Nu is the Nusselt number based on the "entry length".

Since the radiative heat transfer is a small fraction, about 2.4% (h=25 $\text{W m}^{-2}\,\text{K}^{-1}$) and 12.0% (h =5 $\text{W m}^{-2}\,\text{K}^{-1}$), of the total heat dissipated by a slightly larger format cell (26650) battery, the different heat contributions from a cell can be clubbed together as the heat loss and the Enthalapy of the reaction, the above equations reduces to,

$$\frac{dT}{dt} = \frac{I(t)}{C_b} \left(U - V - T \frac{\partial U}{\partial T} \right) - \frac{T - T_{\text{amb}}}{\tau}, \tag{11}$$

where $C_b = m_{\text{cell}} C_p$, U is the open circuit potential (OCP), T_{amb} is the ambient temperature. $T\partial U/\partial T$ is the entropic term, corresponding to the reversible heat generation in the cell, and $\tau = A_{\text{cross}} h_{\text{conv}}/m_{\text{cell}} C_p$, is the cooling rate.

III. Prognostics Architecture

The combined prognostics architecture is shown in Fig. 2. In discrete time k, the system is provided with inputs $\mathbf{u}_k$ that include [P,T] i.e power and temperature and provides measured outputs $\mathbf{y}_k$. The estimation module uses this information, along with the system model, to compute an estimate $p(\mathbf{x}(k), \boldsymbol{\theta}(k)|\mathbf{y}(k_0{:}k))$. The prediction module uses the joint state-parameter distribution and the system model, along with hypothesized future inputs, to compute the probability distribution $p(k_E(k_P)|\mathbf{y}(k_0{:}k_P))$ at given prediction times k_P to estimate both the voltage (V) and temperature (T). As can be seen the upper blocks define state estimation and EOD prediction for a given cycle while the lower block takes in the same information but estimating based on the aging cycle. Hence the single combine framework estimates SOC and Temperature i.e EOD(V,T) for a given cycle while in parallel also predicting EOL (C,T).

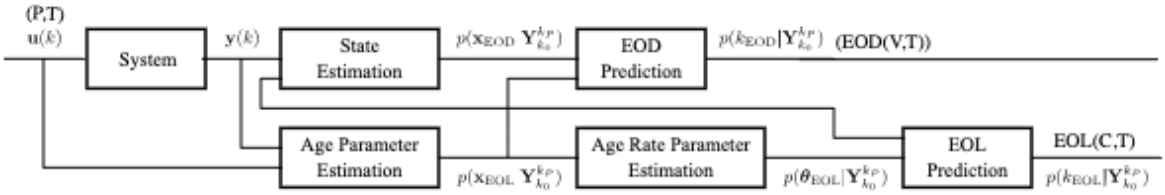

Fig. 2 Prognostics Architecture

In the application of prognostics in this example, we do not account for any uncertainty except for that provided in the state estimate, as our focus is on determining how accurate the model can predict EOD given precise information about the future. A more general prognostics architecture that accounts for these additional sources of uncertainty is described in [17, 18].

IV. Results and Discussion

The thermal model was validated for two case studies in the MATLAB implementation of the framework and then integrated into the ProgPy tool (discussed later). The first case study is lab randomised discharge data set while the second was a simulated flight profile (SFP) for a UAV which is translated from flight tests being done in parallel research work. Each of the case study is discussed in details below with observed results for model validation.

Given an accurate model and knowledge of future system inputs, prognostics should also be precise. This section demonstrates battery prognostics using the novel model introduced in this paper. We employ the architecture outlined in Section III. The unscented Kalman filter (UKF), combined with the battery model, serves as the estimation algorithm discussed in [19, 20] and [17, 21] for details on the implementation to prognostics framework. The UKF operates on a set of deterministic number of selected samples, called *sigma points*, that are used to represent the joint state-parameter distribution $p(\mathbf{x}(k), \boldsymbol{\theta}(k)|\mathbf{y}(k_0{:}k))$.

The prediction algorithm utilizes a simplified simulation as detailed in [22]. Each sigma point is propagated forward using the model until the End of Discharge (EOD) is attained. The resulting EODs for each sigma point are then used to establish the EOD distribution.

A. Case 1

The open source NASA Dataset for Randomised Discharge Data [23] was used to develop and test the thermal model. The dataset consists of about 27 datasets with varying discharge current sampling and environmental conditions. Since the dataset focuses on collecting voltage data for end-of-life (EOL) and state-of-health (SOH) estimation, the thermal data had significant unexplained temperature jumps. To screen for the thermal data that could be used for parameter estimation and then for prognostics, a screening criteria of a goodness fit of with $R^2 > 0.99$, when the cooling curve during the relaxation period is fitted to the convective cooling with the no heat generation. It was observed that the data collected at room temperature yielded reasonable data (about 70%) with the goodness fit beyond 99%. On the other hand, the higher temperature profiles (RW23, RW25, and RW26) were not used due to inconsistent data, and it seems that this inconsistency was due to the sensitivity of the temperature controller in the thermal chamber. Therefore only three profiles were to showcase the proof-of-concept.

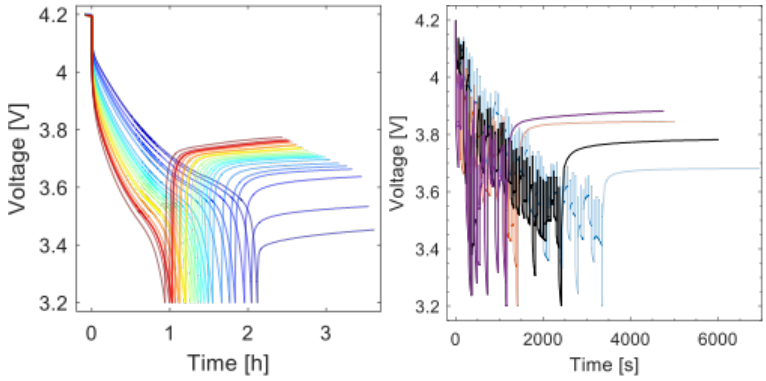

Fig. 3 Dataset includes a) reference discharges and b) random walk discharges. Reference discharge clearly shows three aging parameters: shorter discharges (loss in capacity), larger voltage drop (increase in cell resistance), and rising relaxation voltage (increase in diffusion time) with aging of the battery

Fig.3a and Fig.3b plots show reference (constant current) discharge cycle and random discharge cycles, respectively, for a single cell from the dataset. In addition to this data, temperature data was also collected during the experiments.

A simple current pulse is used to validate the implementation of the thermal model. Since a 5 min 1C pulse occurs around 80% SOC, this allows the temperature of the cell to rise significantly and the enough time for the cell to start cooling (as seen in Fig. 4c). A constant discharge profile with a high current pulse is tested as can be seen from Fig. 4a with the later plots showing respective change in voltage and temperature. As can be observed the pulse does lead to a jump in the temperature profile and tapering back again as the pulse subsides.

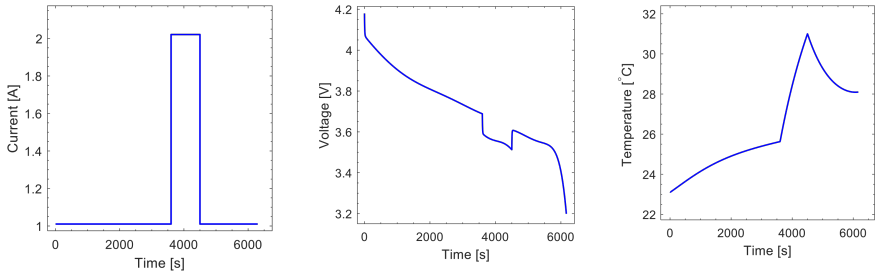

Fig. 4 Single Cell Pulse Discharge Profile

This profile is run through the modeling framework to estimate both the voltage and temperature which is shown in Fig. 5. Note that, in this case, the future inputs (i_{app}) are known, thus the sole uncertainty in the prediction stems from the model itself. A voltage cutoff of $V_{\text{EOD}} = 2.6\ V$ is employed to define EOD.

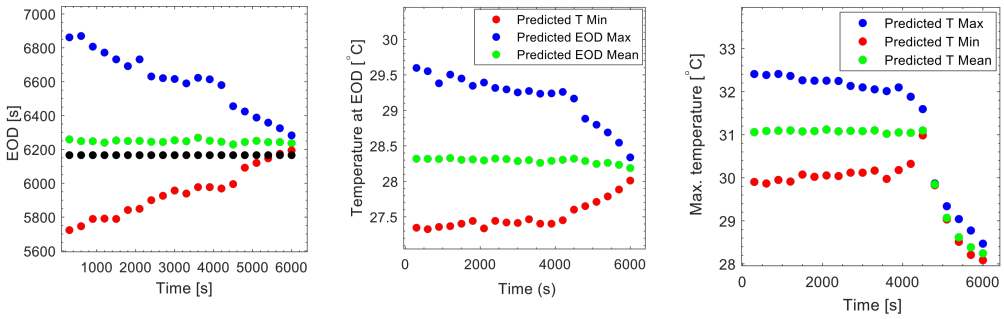

Fig. 5 Single Cell Pulse Discharge Predictions

Figure 5a shows end-of-discharge (EOD) time estimation with uncertainty bounds, while Fig. 5b shows the estimated

temperature at EOD, and Fig. 5c provides estimation for maximum temperature the cell potentially reach provided the given profile. Note that, the estimates of the value and the time of the maximum temperature can help with decision if the current profile exceeds any thermal set limits and if any future change in the discharge profile may be required.

B. Case 2

A Simulated Flight Profile (SFP) was generated using data collected from UAV flight tests in a parallel research program. The SFP is generated to validate the thermal model on operational profiles. The plots in Fig. 6 shows how the current, voltage and temperature change as the flight goes through different phases of a flight: take-off, cruise, package drop, further again gaining altitude, cruse and land back.

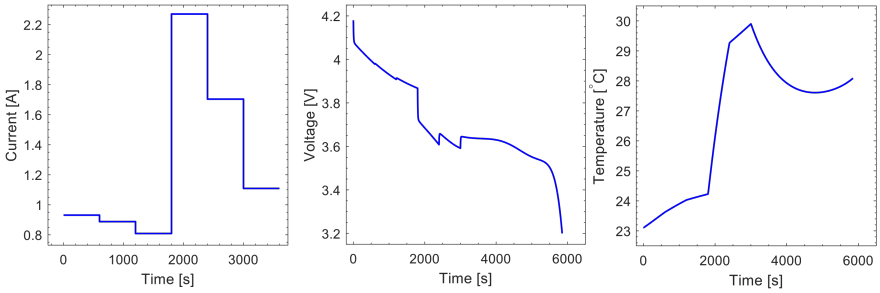

Fig. 6 Current, Voltage and Temperature changes over the Flight Profile

The updated thermal model with fine tuning based on the variable discharge data, then went through the validation step wherein a current profile as shown in Fig. 7 was provided as input and temperature predictions were done at intermediate steps. The average temperature estimate is shown by the line in the center with a uncertainty boundary around.

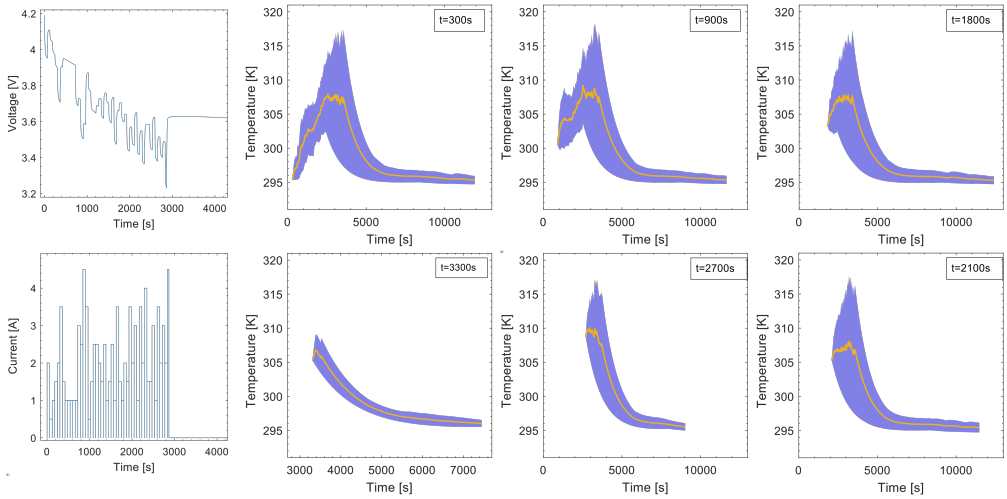

Fig. 7 Thermal Predictions at various time-steps in the discharge cycle

As can be seen in the early steps bounds are larger around peak temperature values, since the model estimates a looking forward and estimating the temperature with higher uncertainty which improves (uncertainty reduces) near the end-of-discharge, as the discharge time passes the high current region near the end, which is different from Figs. 4 and 6 where the current peaks near the middle of the discharge profile. Thus in Fig.7 the model compensate for all the thermodynamics within the cell as current changes until near the end-of-discharge.

Fig. 8 compares the performance of the prognostics algorithm based on selection of the temperature metric: T_{EOD} or T_{max}. Estimation of the EOD temperature allows for making arrangements for better cooling on arrival or changes to the turn around time for batteries to be safe for next flight, or safe-to-charge. Since this work stresses on validation

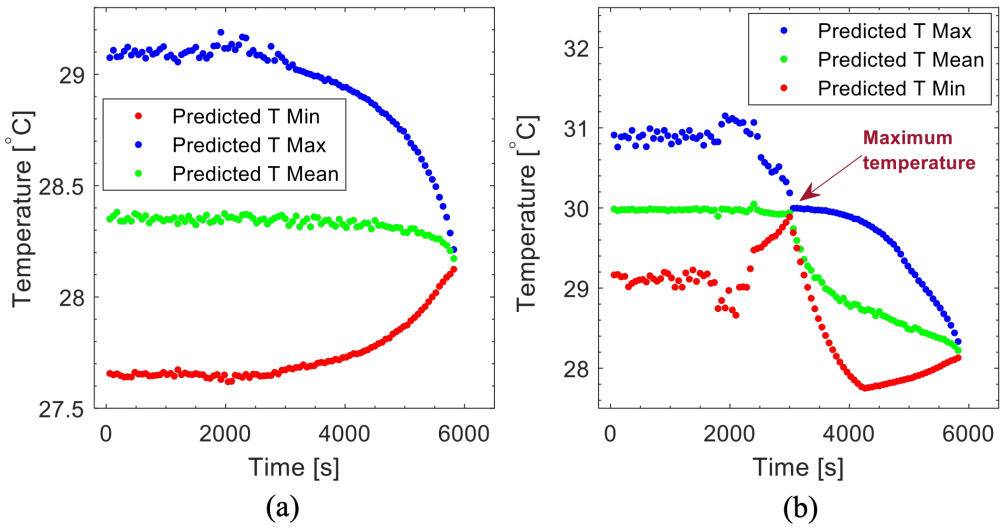

Fig. 8 Thermal Future estimate for (a) end-of-flight (EOF) for the SFP and (b) Max temperature reached for SFP

of the thermal model the later plot in shows the predictions results for the SFP. This includes the min, max values to include the uncertainty prediction bounds. The plot (a) in Fig.8 show estimated temperature that the cell may reach at the end of the SFP while (b) shows how max temperature reached and then tapering of the temperature once the SFP ends while the current to the battery model is close to zero, indicating a cooling down effect.

V. ProgPy

The Prognostics Python Package (ProgPy) is a versatile tool designed to support research and applications in systems health management for engineering systems. It provides a comprehensive framework for defining, building, and evaluating prognostic models. Additionally, ProgPy offers a collection of developed models for specific components and sub-systems, streamlining the development process for researchers.

By combining these models with its state estimation and prediction capabilities, ProgPy empowers researchers to explore and develop advanced prognostics methods. This open-source toolkit fosters collaboration and innovation in the field of systems health management, making it a valuable resource for both academic research and practical applications [24].

Prognostic model inputs represent the controllable factors that influence a system's behavior and progression. Each model's 'inputs' property specifies the expected inputs, such as applied current (i) in the case of a battery. Environmental conditions like temperature or pressure can also be considered inputs, affecting the system's overall state. Inputs are one of the inputs to the state transition model, described in States.

ProgPy prognostic models are state-transition models. The internal state of the system at any time is represented by one or more (frequently hidden) state variables, represented by the custom type StateContainer. Each model has a discrete set of states, the keys of which are defined by the states property.

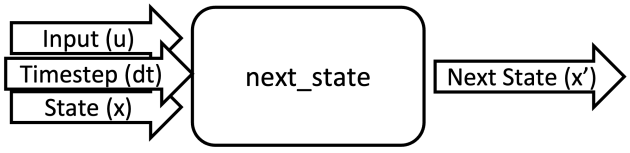

Fig. 9 State Transition [24]

Outputs are measurable quantities within a system that are directly related to its state update. In the context of prognostics, these outputs are typically the aspects that are being monitored or observed. State estimators leverage

the discrepancy between predicted and measured values of these outputs to accurately estimate the system's current condition. This process enables the model to make informed predictions about future behavior and potential failures.

Outputs are a function of only the system state (x) and parameters (Θ). The expected outputs for a model are defined by its outputs property. The logic of calculating outputs from system state is provided by the user in the model progpy.PrognosticsModel.output() method.

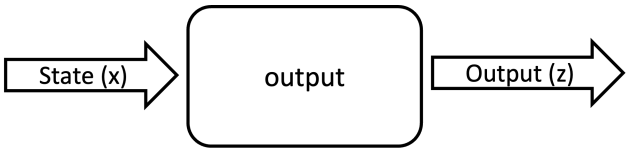

Fig. 10 Output [24]

The existing ProgPy model was updated to integrate the existing li-ion battery model to include the thermal model as discussed in section II.C. The updated thermal model has the ability to estimate the current temperature as well was prognose the further thermal rate based on loading profiles. This is discussed further in the next section.

VI. Conclusion

This work presents integration of a physics-based thermal prediction model into the earlier developed electrochemistry model [11]. By integrating thermal capability, the enhanced battery model can now estimate End of Discharge (EOD) as well as predict both State of Charge (SOC) and temperature for a single 18650 cell based on future loading. This capability to forecast SOC and temperature can be effectively incorporated into a decision-making framework. This framework can further limit operation when the battery is likely to enter thermal runaway conditions, such as when temperatures exceeds a defined threshold due to specific future operational tasks.

The updated model's validation was comprehensive, encompassing two case studies. Initially, it was tested on a single constant discharge profile, accurately predicting both the End of Discharge (EOD) and future temperature evolution. This confirmed its effectiveness under constant loading conditions. Using the same data, we subsequently validated the model's performance was evaluated against variable discharge profiles sourced from a publicly available datasets. This broader range of conditions tested its adaptability and robustness in real-world scenarios with fluctuating loading profiles. In the second case study, a simulated-flight-profile (SPF) for a single 18650 cell was employed to assess the model's accuracy under the unique stresses and variations experienced during flight operations. The model's ability to maintain accurate predictions of SOC and temperature throughout this profile underscored its potential for use in aviation applications.

Having undergone this rigorous validation process, the model was deemed suitable for integration into the ProgPy toolkit. This open-source platform provides researchers and engineers with a valuable tool for battery prognostics, facilitating further advancements in battery management and optimization [24].

In this research focus was on modeling for a single 18650 cell, but research is underway to expand this model to encompass multiple cells and larger battery packs. This is crucial for real-world applications, as most devices utilize battery packs rather than individual cells. Initial findings in this area are detailed in [25], highlighting the progress and potential of this research direction towards battery pack-level system health monitoring.

Furthermore, parallel research work is under investigation to leverage prognostic information generated by varying fidelity of battery models. This information, such as predicted State of Charge (SOC) and temperature, can be instrumental in making informed decisions and optimizing scheduling for various applications, particularly in the realm of autonomous systems. The integration of accurate battery prognostics with decision-making algorithms holds significant promise for enhancing the efficiency, safety, and longevity of battery-powered autonomous vehicles.

Acknowledgments

This work was authored by employees of KBR Wyle Services, LLC under Contract No. 80ARC020D0010 with the National Aeronautics and Space Administration. The United States Government retains and the publisher, by accepting the article for publication, acknowledges that the United States Government retains a non-exclusive, paid-up, irrevocable, worldwide license to reproduce, prepare derivative works, distribute copies to the public, and perform publicly and display publicly, or allow others to do so, for United States Government purposes. All other rights are reserved by the

copyright owner.

References

[1] Bosson, C., and Lauderdale, T. A., "Simulation evaluations of an autonomous urban air mobility network management and separation service," *2018 Aviation Technology, Integration, and Operations Conference*, 2018, p. 3365. https://doi.org/10.2514/6.2018-3365.

[2] Pradeep, P., and Wei, P., "Energy-efficient arrival with rta constraint for multirotor evtol in urban air mobility," *Journal of Aerospace Information Systems*, Vol. 16, No. 7, 2019, pp. 263–277.

[3] Thipphavong, D. P., and et al, "Urban air mobility airspace integration concepts and considerations," *2018 Aviation Technology, Integration, and Operations Conference*, 2018, p. 3676. https://doi.org/10.2514/6.2018-3676.

[4] Deng, J., Bae, C., Marcicki, J., Masias, A., and Miller, T., "Safety modelling and testing of lithium-ion batteries in electrified vehicles," *Nature Energy*, Vol. 3, No. 4, 2018, pp. 261–266. https://doi.org/10.1038/s41560-018-0122-3.

[5] Coman, P. T., Darcy, E. C., Veje, C. T., and White, R. E., "Numerical analysis of heat propagation in a battery pack using a novel technology for triggering thermal runaway," *Applied Energy*, Vol. 203, 2017, pp. 189–200. https://doi.org/10.1016/j.apenergy.2017.06.033.

[6] Coman, P. T., Darcy, E. C., Strangways, B., and White, R. E., "A Reduced-Order Lumped Model for Li-Ion Battery Packs during Operation," *Journal of The Electrochemical Society*, Vol. 168, No. 10, 2021, p. 100525. https://doi.org/10.1149/1945-7111/ac2dcb.

[7] Coman, P. T., Darcy, E. C., and White, R. E., "Simplified Thermal Runaway Model for Assisting the Design of a Novel Safe Li-Ion Battery Pack," *Journal of The Electrochemical Society*, Vol. 169, No. 4, 2022, p. 040516. https://doi.org/10.1149/1945-7111/ac62bd.

[8] Doo, J., Pavel, M., Didey, A., Hange, C., Diller, N., Tsairides, M., Smith, M., Bennet, E., Bromfield, M., and Mooberry, J., *NASA Electric Vertical Takeoff and Landing (eVTOL) Aircraft Technology for Public Services–A White Paper: NASA Transformative Vertical Flight Working Group 4 (TVF4)*, NASA, 2021.

[9] Daigle, M., and Kulkarni, C., "Electrochemistry-based Battery Modeling for Prognostics," *Annual Conference of the Prognostics and Health Management Society 2013*, 2013, pp. 249–261.

[10] Hogge, E., Bole, B., Vazquez, S., Kulkarni, C., Strom, T., Hill, B., Smalling, K., and Quach, C., "Verification of Prognostic Algorithms to Predict Remaining Flying Time for Electric Unmanned Vehicles," *International Journal of Prognostics and Health Management, ISSN 2153-2648, 2018 021*, 2018.

[11] Daigle, M., and Kulkarni, C. S., "Electrochemistry-based Battery Modeling for Prognostics," *Annual Conference of the Prognostics and Health Management Society*, Vol. 4, 2013, p. 13.

[12] Kriston, A., Podias, A., Adanouj, I., and Pfrang, A., "Analysis of the Effect of Thermal Runaway Initiation Conditions on the Severity of Thermal Runaway-Numerical Simulation and Machine Learning Study," *Journal of the Electrochemical Society*, Vol. 167, 2020, p. 090555. https://doi.org/10.1149/1945-7111/ab9b0b.

[13] Paul, C., "Thermal analysis predictions for scale-up from 18650 to 21700," , nov 2022.

[14] Kim, G.-H., Pesaran, A., and Spotnitz, R., "A three-dimensional thermal abuse model for lithium-ion cells," *Journal of Power Sources*, Vol. 170, No. 2, 2007, pp. 476–489. https://doi.org/10.1016/j.jpowsour.2007.04.018.

[15] Hatchard, T. D., MacNeil, D. D., Stevens, D. A., Christensen, L., and Dahn, J. R., "Importance of Heat Transfer by Radiation in Li - Ion Batteries during Thermal Abuse," *Electrochemical and Solid-State Letters*, Vol. 3, No. 7, 2000, p. 305. https://doi.org/10.1149/1.1391131.

[16] Guo, M., Sikha, G., and White, R. E., "Single-Particle Model for a Lithium-Ion Cell: Thermal Behavior," *Journal of The Electrochemical Society*, Vol. 158, No. 2, 2010, p. A122. https://doi.org/10.1149/1.3521314.

[17] Daigle, M., Saxena, A., and Goebel, K., "An Efficient Deterministic Approach to Model-based Prediction Uncertainty Estimation," *Annual Conference of the Prognostics and Health Management Society*, 2012, pp. 326–335.

[18] Sankararaman, S., Daigle, M., Saxena, A., and Goebel, K., "Analytical Algorithms to Quantify the Uncertainty in Remaining Useful Life Prediction," *Proceedings of the 2013 IEEE Aerospace Conference*, 2013.

[19] Julier, S. J., and Uhlmann, J. K., "A new extension of the Kalman filter to nonlinear systems," *Proceedings of the 11th International Symposium on Aerospace/Defense Sensing, Simulation and Controls*, 1997, pp. 182–193.

[20] Julier, S. J., and Uhlmann, J. K., "Unscented filtering and nonlinear estimation," *Proceedings of the IEEE*, Vol. 92, No. 3, 2004, pp. 401–422.

[21] Daigle, M., Saha, B., and Goebel, K., "A comparison of filter-based approaches for model-based prognostics," *Proceedings of the 2012 IEEE Aerospace Conference*, 2012.

[22] Daigle, M., and Goebel, K., "Model-based Prognostics with Concurrent Damage Progression Processes," *IEEE Transactions on Systems, Man, and Cybernetics: Systems*, Vol. 43, No. 4, 2013, pp. 535–546.

[23] Bole, B., Kulkarni, C. S., and Daigle, M., "Randomized Battery Usage Data Set," , 2014. URL https://www.nasa.gov/content/prognostics-center-of-excellence-data-set-repository.

[24] Teubert, C., Griffith, K. J., Corbetta, M., Kulkarni, C., Banerjee, P., Watkins, J., and Daigle, M., "ProgPy Python Prognostics Packages," , Oct. 2023. URL https://nasa.github.io/progpy.

[25] Khasin, M., Mehta, M. R., Kulkarni, C., and Lawson, J. W., "Thermal data-driven model reduction for enhanced battery health monitoring," *Journal of Power Sources*, Vol. 604, 2024, p. 234442. https://doi.org/https://doi.org/10.1016/j.jpowsour.2024.234442, URL https://www.sciencedirect.com/science/article/pii/S0378775324003938.